Inorganic Chemistry
Article

Inorg. Chem. **2009**, *48*, 11407–11414 **11407**
DOI: 10.1021/ic901523u

Probing the Excited State Properties of the Highly Phosphorescent Pt(dpyb)Cl Compound by High-Resolution Optical Spectroscopy

Andreas F. Rausch,[†] Lisa Murphy,[‡] J. A. Gareth Williams,*[,‡] and Hartmut Yersin*[,†]

[†]*Universität Regensburg, Institut für Physikalische und Theoretische Chemie, 93053 Regensburg, Germany, and* [‡]*Department of Chemistry, University of Durham, Durham, DH1 3LE, U.K.*

Received July 31, 2009

Detailed photophysical studies of the emitting triplet state of the highly phosphorescent compound Pt(dpyb)Cl based on high-resolution optical spectroscopy at cryogenic temperatures are presented {dpyb = N^C^2^N-coordinated 1,3-di(pyridylbenzene)}. The results reveal a total zero-field splitting of the emitting triplet state T_1 of 10 cm^{-1} and relatively short individual decay times for the two higher lying T_1 substates II and III, while the decay time of the lowest substate I is distinctly longer. Further evidence for the assignment of the T_1 substates is gained by emission measurements under high magnetic fields. Distinct differences are observed in the vibrational satellite structures of the emissions from the substates I and II, which are dominated by Herzberg−Teller and Franck−Condon activity, respectively. At T=1.2 K, the individual spectra of these two substates can be separated by time-resolved spectroscopy. For the most prominent Franck−Condon active modes, Huang−Rhys parameters of $S \approx 0.1$ can be determined, which are characteristic of very small geometry rearrangements between the singlet ground state and the triplet state T_1. The similar geometries are ascribed to the high rigidity of the Pt(N^C^N) system which, unlike complexes incorporating bidentate phenylpyridine-type ligands and exhibiting similar metal-to-ligand charge transfer admixtures, cannot readily distort from planarity. The results provide new insight into strategies for optimizing the performance of platinum-based emitters for applications such as organic light-emitting diode (OLED) technology and imaging.

1. Introduction

Phosphorescent transition metal complexes that emit efficiently from triplet excited states are the subject of a great deal of attention. Much of this interest over the past decade has been driven by research into the new generation of display screen technology, organic light-emitting diodes (OLEDs), which can benefit from the incorporation of such materials to induce emission from otherwise wasted triplet states.[1−5] The recombination of charge carriers within an electroluminescent device leads to triplet and singlet excitons in a ratio as high as 3:1.[6−8] In a device comprised of a purely organic emitting material, emission from the triplet states is spin-forbidden with a very low probability (radiative rate constants k_r of only around 1 s^{-1}), limiting the maximum achievable internal efficiencies to 25%. In contrast, in third-row transition metal complexes, strong spin−orbit coupling (SOC) induced by the metal ion can promote the radiative decay of the triplet state; for example, k_r may be increased to the order of 10^6 s^{-1}. Intersystem crossing from higher-lying singlet states is also promoted, so that the singlet states are utilized too, and thus, all excitons are potentially converted into light. On the other hand, the resulting phosphorescence lifetimes of the triplet excited states of such complexes, of the order of microseconds, are sufficiently long compared to fluorescence lifetimes of organic molecules (typically 1−10 ns) to allow them to be employed in sensing and imaging applications that make use of time-resolved detection procedures.[9−11] These techniques offer not only a means of discriminating from short-lived background emission to improve sensitivity, but also the possibility of using lifetimes

*To whom correspondence should be addressed. E-mail: hartmut.yersin@chemie.uni-regensburg.de (H.Y.); j.a.g.williams@durham.ac.uk (J.A.G.W.).

(1) Yersin, H., Ed. *Highly Efficient OLEDs with Phosphorescent Materials*; Wiley-VCH: Weinheim, 2008.
(2) Evans, R. C.; Douglas, P.; Winscom, C. J. *Coord. Chem. Rev.* **2006**, *250*, 2093.
(3) Polikarpov, E.; Thompson, M. E. *Mater. Matters* **2007**, *2*(3), 21.
(4) Williams, J. A. G.; Develay, S.; Rochester, D. L.; Murphy, L. *Coord. Chem. Rev.* **2008**, *252*, 2596.
(5) Chou, P. T.; Chi, Y. *Chem.—Eur. J.* **2007**, *13*, 380.
(6) For an introduction to the principles of OLEDs and their operation, see, for example: Hung, L. S.; Chen, C. H. *Mater. Sci. Eng. R* **2002**, *39*, 143.
(7) Baldo, M. A.; O'Brien, D. F.; Thompson, M. E.; Forrest, S. R. *Phys Rev. B* **1999**, *60*, 14422.
(8) Yersin, H. *Top. Curr. Chem.* **2004**, *241*, 1.
(9) Lakowicz, J. R. *Principles of Fluorescence Spectroscopy*, 3rd ed.; Springer: New York, 2006; Chapters 20 and 22.
(10) Botchway, S. W.; Charnley, M.; Haycock, J. W.; Parker, A. W.; Rochester, D. L.; Weinstein, J. A.; Williams, J. A. G. *Proc. Natl. Acad. Sci. U.S.A.* **2008**, *105*, 16071.
(11) Mak, C. S. K.; Pentlehner, D.; Stich, M.; Wolfbeis, O. S.; Chan, W. K.; Yersin, H. *Chem. Mater.* **2009**, *21*, 2173.

Published on Web 10/30/2009

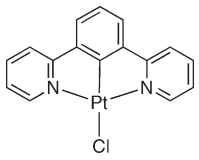

Figure 1. Structure of Pt(dpyb)Cl.

as a reporter parameter, in contrast to intensity or wavelength.

We have been exploring the chemistry of platinum(II) complexes with terdentate cyclometalating ligands based on 1,3-di(2-pyridyl)benzene (dpybH), which offer the metal ion an N^C^N coordination environment (Figure 1).[12,13]

These compounds are among the brightest known Pt-based emitters in solution at room temperature;[14] e.g. for Pt(dpyb)Cl, $\Phi_{PL} = 0.60$ and $\tau = 7.2$ μs in deoxygenated dichloromethane. The complexes are thermally stable and sublimable, rendering them suitable for vacuum deposition into OLED structures. High device efficiencies have been obtained in this way,[15,16] and the color can be tuned widely according to ligand substituents. Moreover, the excimers and/or aggregates formed by these complexes emit intensely in the red-to-near-infrared (NIR) region of the spectrum.[12,13,17] The use of a thin film of the pure compounds as an emissive layer in an OLED structure leads to NIR-emitting devices with external quantum efficiencies as high as 10.7% photons/electron.[18] The balance of emission from the monomeric and aggregate emission bands in a doped emissive layer can be tuned, according to doping concentration, to give white-light-emitting devices (e.g., at 15% doping by mass, CIE = 0.40, 0.43 and efficiency = 15.5% photons/electron).[19,20] Such systems also offer promise as efficient growth lights in horticulture, owing to the close match of the bimodal-like emission profile with the absorption spectra of green plants.[21]

Very recently, the same class of complexes has also been used for time-resolved imaging in live cells.[10] The features that make the complexes suitable for use in OLEDs also prove to be attractive for this purpose: their low molecular weight, charge-neutrality, and lipophilic character facilitate rapid diffusion-controlled passage through the cell membrane, while the bright emission and lifetimes of the order of a microsecond, even in the presence of oxygen, allow time-gated images to be readily acquired. Other applications of these compounds have included oxygen sensors;[22] metal ion sensors in which emission is modulated in response to ion binding;[23] derivatives with long alkyl chains in which the emission is a function of the liquid crystallinity;[24] and mechanochromic complexes in which the color of solid-state emission is influenced by grinding.[25]

The high emission efficiency of these complexes must arise from a combination of minimal nonradiative decay and spin−orbit coupling favoring the triplet radiative decay.[14,26,27] Typically, SOC is efficient in complexes with emitting states of metal-to-ligand charge transfer (MLCT) character,[8,26,27] owing to the greater participation of the metal than in ligand-centered (LC) states.[26−29] However, the emission of Pt(dpyb)Cl and most of its derivatives, at least at first sight, appears to display features more typical of LC transitions (see below). Moreover, it has been shown that SOC depends on a compound's coordination geometry and is frequently more efficient in 6-coordinate than in comparable 4-coordinate complexes {e.g. Ir(III) vs Pt(II)}.[26,27,29−31] Clearly, the nature of the emitting states of these complexes merits a more detailed investigation. In this contribution, we probe the emitting triplet state of Pt(dpyb)Cl by means of high-resolution emission and excitation spectroscopy at cryogenic temperatures and in the presence of external magnetic fields. The zero-field splitting of the T_1 state, the individual deactivation rates of the three triplet substates, and the vibrational satellite structures in emission are investigated to provide further insight into the nature of the emitting state, which governs the intense luminescence of this class of complexes with diverse applications.

2. Experimental Section

1,3-Di(2-pyridyl)benzene (dpybH) was prepared by palladium-catalyzed reaction of 2-(tributylstannyl)-pyridine with 1,3-dibromobenzene. Its platinum(II) complex was formed upon reaction of the ligand with K_2PtCl_4 in acetic acid, followed by extraction into dichloromethane, as described previously.[12] Emission spectra at 300 and 77 K were measured using a Jobin Yvon FluoroMax-2 spectrofluorimeter, fitted with a red-sensitive Hamamatsu R928 photomultiplier tube. Samples were degassed by a minimum of three freeze−pump−thaw cycles to base pressures of $< 5 \times 10^{-2}$ mbar at 77 K. For investigations at low temperature, Pt(dpyb)Cl

(12) Williams, J. A. G.; Beeby, A.; Davies, E. S.; Weinstein, J. A.; Wilson, C. *Inorg. Chem.* **2003**, *42*, 8609.
(13) Farley, S. J.; Rochester, D. L.; Thompson, A. L.; Howard, J. A. K.; Williams, J. A. G. *Inorg. Chem.* **2005**, *44*, 9690.
(14) For a review of luminescent Pt(II) complexes: Williams, J. A. G. *Top. Curr. Chem.* **2007**, *281*, 205.
(15) Sotoyama, W.; Satoh, T.; Sawatari, N.; Inoue, H. *Appl. Phys. Lett.* **2005**, *86*, 153505.
(16) (a) Cocchi, M.; Virgili, D.; Fattori, V.; Rochester, D. L.; Williams, J. A. G. *Adv. Funct. Mater.* **2007**, *17*, 285. (b) Kalinowski, J.; Cocchi, M.; Virgili, D.; Fattori, V.; Williams, J. A. G. *Chem. Phys. Lett.* **2006**, *432*, 110. (c) Virgili, D.; Cocchi, M.; Fattori, V.; Sabatini, C.; Kalinowski, J.; Williams, J. A. G. *Chem. Phys. Lett.* **2006**, *433*, 145.
(17) Develay, S.; Williams, J. A. G. *Dalton Trans.* **2008**, 4562.
(18) (a) Cocchi, M.; Virgili, D.; Fattori, V.; Williams, J. A. G.; Kalinowski, J. *Appl. Phys. Lett.* **2007**, *90*, 023506. (b) Cocchi, M.; Kalinowski, J.; Virgili, D.; Williams, J. A. G. *Appl. Phys. Lett.* **2008**, *92*, 113302.
(19) (a) Cocchi, M.; Kalinowski, J.; Virgili, D.; Fattori, V.; Develay, S.; Williams, J. A. G. *Appl. Phys. Lett.* **2007**, *90*, 163508. (b) Kalinowski, J.; Cocchi, M.; Virgili, D.; Fattori, V.; Williams, J. A. G. *Adv. Mater.* **2007**, *19*, 4000.
(20) Other examples of white light-emitting diodes using monomer and aggregate emission from N^C-coordinated platinum complexes have been described previously: (a) Adamovich, V.; Brooks, J.; Tamayo, A.; Alexander, A. M.; Djurovich, P. I.; D'Andrade, B. W.; Adachi, C.; Forrest, S. R.; Thompson, M. E. *New J. Chem.* **2002**, *26*, 1171. (b) Williams, E. L.; Haavisto, K.; Li, J.; Jabbour, G. E. *Adv. Mater.* **2007**, *19*, 197.
(21) Fattori, V.; Williams, J. A. G.; Murphy, L.; Cocchi, M.; Kalinowski, J. *Photon. Nanostruct. Fundam. Appl.* **2008**, *6*, 225.
(22) Evans, R. C.; Douglas, P.; Williams, J. A. G.; Rochester, D. L. *J. Fluorescence* **2006**, *16*, 201.
(23) Rochester, D. L.; Develay, S.; Záliš, S.; Williams, J. A. G. *Dalton Trans.* **2009**, 1728.
(24) Kozhevnikov, V. N.; Donnio, B.; Bruce, D. W. *Angew. Chem., Int. Ed.* **2008**, *47*, 6286.
(25) Abe, T.; Itakura, T.; Ikeda, N.; Shinozaki, K. *Dalton Trans.* **2009**, 711.
(26) Rausch, A. F.; Homeier, H. H. H.; Yersin, H. In *Topics in Organometallic Chemistry - Photophysics of Organometallics*; Lees, A. J., Ed.; Springer: Berlin/Heidelberg, *29*, 2010
(27) Yersin, H.; Finkenzeller, W. J. In *Highly Efficient OLEDs with Phosphorescent Materials*; Yersin, H., Ed.; Wiley-VCH: Weinheim, 2008, 1.
(28) Yersin, H.; Donges, D. *Top. Curr. Chem.* **2001**, *214*, 81.
(29) Rausch, A. F.; Homeier, H. H. H.; Djurovich, P. I.; Thompson, M. E.; Yersin, H. *Proc. SPIE* **2007**, 66550F.
(30) Wilson, M. H.; Ledwaba, L. P.; Field, J. S.; McMillin, D. R. *Dalton Trans.* **2005**, 2754.
(31) Siddique, Z. A.; Yamamoto, Y.; Ohno, T.; Nozaki, K. *Inorg. Chem.* **2003**, *42*, 6366.

Table 1. Photophysical Data of Pt(dpyb)Cl at 300 K in CH_2Cl_2 Except Where Stated Otherwise[a]

absorbance λ_{max}/nm (ε M^{-1} cm^{-1})	332 (6510), 380 (8690), 401 (7010)[b], 454 (270), 485 (240)[c]
emission λ_{max}/nm	491, 524, 562
Φ_{PL} degassed (aerated)	0.60 (0.039)[d]
τ_0 degassed (aerated)/μs[e]	7.2 (0.5)
τ at 77 K/μs[f]	7.0

[a] Data from ref 12. [b] Lowest energy singlet band. [c] Lowest energy triplet band. [d] Obtained using fluorescein, quinine sulfate, and $Ru(bpy)_3Cl_2$ as three independent standards. [e] τ_0 is the lifetime at infinite dilution obtained from the concentration dependence of the decay rate constant; estimated uncertainty ±10%. [f] In diethyl ether/isopentane/ethanol (2:2:1 by volume).

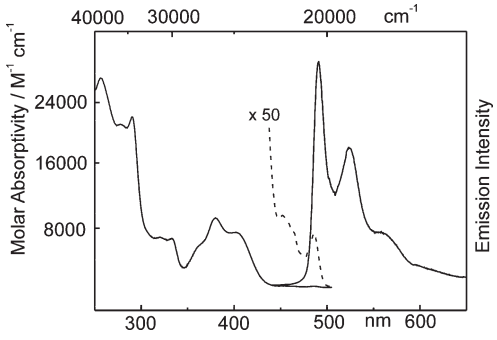

Figure 2. Absorption and emission spectra of Pt(dpyb)Cl in CH_2Cl_2 solution at 300 K (λ_{exc} = 400 nm). The low-energy portion of the absorption spectrum is shown on an expanded scale (×50) to highlight the $S_0 \rightarrow T_1$ transition and the small Stokes shift.

was dissolved in *n*-octane at a concentration of ≈10^{-5} mol/L. The measurements were carried out in a He cryostat (Cryovac Konti Cryostat IT) in which the He gas flow, He pressure, and heating were controlled. For magnetic field experiments, an Oxford Instruments MD10 cryostat equipped with a 12 T magnet was used. A pulsed Nd:YAG laser (IB Laser Inc., DiNY pQ 02) with a pulse width of about 7 ns was applied as the excitation source for emission spectra and lifetime measurements, using the third harmonic at 355 nm (28170 cm^{-1}). For measurements of excitation spectra, a pulsed dye laser (Lambdaphysik Scanmate 2C) with Coumarin 102 was operated. The spectra were recorded with an intensified CCD camera (Princeton PIMAX) or a cooled photomultiplier (RCA C7164R) attached to a triple spectrograph (S&I Trivista TR 555). Time-resolved emission spectra were recorded with a gated photon counter (Stanford Research Systems, Model SR 400). Decay times were registered using a FAST Comtec multichannel scaler PCI card with a time resolution of 250 ps.

3. Results and Discussion

3.1. Photophysical Properties at Room Temperature and at 77 K. Key photophysical properties of Pt(dpyb)Cl at 300 K are summarized in Table 1, and the corresponding absorption and emission spectra are shown in Figure 2.

The intense high-energy absorption bands below ≈300 nm can also be found in the absorption spectrum of the free dpybH ligand[32] and thus can be assigned to correspond largely to transitions to ligand-centered (LC) singlet states. The absorption envelope in the region 350−440 nm apparently comprises at least three absorption bands, the lowest energy of which, presumed to be the S_1 state, exhibits pronounced negative solvatochromic behavior.[12] This would suggest a significant degree of charge-transfer character (though not necessarily MLCT) to this singlet state transition. Two very weak but better resolved bands at lower energy (450−495 nm) are attributed to direct absorptions of the T_1 state, facilitated by SOC associated with the Pt(II) ion. These bands are much less solvatochromic than the $S_0 \rightarrow S_1$ band.[12,32] The emission spectrum is structured. At room temperature, the highest energy emission peak and the lowest energy absorption peak exhibit a Stokes shift of 250 cm^{-1}. As for $S_0 \rightarrow T_1$ in absorption, the emission bands display only weak negative solvatochromism.

Upon the basis of the structured profile of the emission spectrum and the small Stokes shift at T = 300 K, we previously assigned the emission from this complex to a state of predominant ^{3}LC ($^3\pi\pi^*$) character.[12] Certainly, the form of the spectrum is very different from the broad, largely featureless profiles typically observed for classic MLCT emitters such as $Ir(ppy)_3$,[27,33] Ir(4,6-dFppy)$_2$(pic),[34] Ir(4,6-dFppy)$_2$(acac),[35] or for neutral iridium complexes containing the dpyb ligand.[36] On the other hand, there must be a considerable contribution from the metal orbitals to the excited state, in order to induce the SOC necessary to promote the triplet radiative decay constant to give a lifetime as short as 7 μs. Such an interpretation is supported by the DFT calculations of Sotoyama et al., who modeled Pt(dpyb)Cl in the gas phase.[32] They estimated that the T_1 and S_1 states have 25% and 32% dπ^* character, respectively. Interestingly, these theoretical results on the molecular orbitals involved also help to account for the different degrees of solvatochromism between the triplet and singlet transitions, since the latter involves a larger redistribution of charge along the Cl−Pt−C axis, strongly perturbing the dipole moment, while the former involves movement of charge "outwards" from this axis, with lesser influence on the dipole moment. Related calculations by Záliš, which take into account the influence of the solvent, have also revealed significant metal participation, not only in the HOMO but also in the LUMO.[23]

At 77 K, the emission spectrum is very similar to that at room temperature. Likewise, the lifetime measured at 77 K in a diethyl ether/isopentane/ethanol (2:2:1) glass is 7.0 μs, the same, within the uncertainty of the measurement, as the value extrapolated to infinite dilution in CH_2Cl_2 at 300 K. The lack of significant changes in the spectra and lifetimes over this temperature range of more than 200 K highlights the extraordinary rigidity of the

(32) Sotoyama, W.; Satoh, T.; Sato, H.; Matsuura, A.; Sawatari, N. *J. Phys. Chem. A* **2005**, *109*, 9760.

(33) Finkenzeller, W. J.; Yersin, H. *Chem. Phys. Lett.* **2003**, *377*, 299.

(34) Rausch, A. F.; Thompson, M. E.; Yersin, H. *Inorg. Chem.* **2009**, *48*, 1928.

(35) Rausch, A. F.; Thompson, M. E.; Yersin, H. *J. Phys. Chem A.* **2009**, *113*, 5927.

(36) (a) Wilkinson, A. J.; Puschmann, H.; Howard, J. A. K.; Foster, C. E.; Williams, J. A. G. *Inorg. Chem.* **2006**, *45*, 8685. (b) Williams, J. A. G.; Wilkinson, A. J.; Whittle, V. L. *Dalton Trans.* **2008**, 2081.

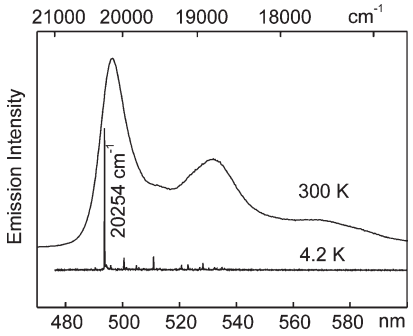

Figure 3. Comparison of the emission spectra of Pt(dpyb)Cl in *n*-octane at $T = 300$ K and at $T = 4.2$ K.

molecule, minimizing nonradiative decay, and the influence of the cyclometalation in displacing potentially deactivating metal-centered dd* states to high energies, out of reach at room temperature.

3.2. High-Resolution Spectroscopy at Cryogenic Temperatures. The emission spectra at room temperature and at 77 K allow only a crude characterization of the emitting triplet state. Therefore, the compound was dissolved in *n*-octane at low concentration and cooled to liquid helium temperatures. In the polycrystalline alkane matrix, the guest molecules (dopants) substitute host molecules and thus lie at defined positions.[28] In suitable cases, the application of this so-called Shpol'skii technique[37] results in highly resolved spectra with line widths of only a few cm^{-1} due to a residual inhomogeneity.[28,38] The obtained line widths are a factor of 100 smaller than those usually obtained with amorphous or glassy host materials. Frequently, the obtained spectra in Shpol'skii matrices represent superpositions of spectra stemming from several sites. In these cases, the investigation of just one specific site is possible by selective excitation with a tunable dye laser. However, in the case of Pt(dpyb)Cl, a very favorable situation is found, since, even under unselective UV excitation, almost all dopant molecules occupy just one site. In Figure 3, the emission spectra of the compound dissolved in *n*-octane at temperatures of 300 and 4.2 K are compared to demonstrate the impressive line narrowing effect achieved by the Shpol'skii technique.

The ambient temperature spectrum consists, as discussed above, of overlapping and relatively broad bands with halfwidths of about 500 cm^{-1}, while the emission spectrum at $T = 4.2$ K exhibits narrow lines with halfwidths of only 4 cm^{-1}. It will be shown below that the most intense line in the highly resolved spectrum depicted in Figure 3, which has its maximum at 20254 cm^{-1}, mainly represents the electronic 0−0 transition from one specific substate of T_1, denoted as substate II, to the singlet ground state S_0. The lines of minor intensity correspond to vibrational satellites stemming from ground state modes. A detailed investigation of the vibrational satellite structure will be carried out in section 3.5.

3.3. Electronic 0−0 Transitions. In order to gain a deeper insight into the properties of the emitting triplet state, emission and excitation measurements were carried out at different temperatures (Figure 4) and under application of external magnetic fields (Figure 5). These experiments allow us to identify the three T_1 substates, denoted as I, II, and III. At zero magnetic field, the lines stemming from the high-energy substates II and III, lying at 20254 cm^{-1} and 20258 , respectively, can be observed in excitation and are in resonance (no Stokes shift) with corresponding emission peaks (Figure 4).

An intensity ratio for the excitation peaks of Int(0 → II)/Int(0 → III) = 2.3 is found, which displays the ratio of the oscillator strengths of the corresponding transitions. In accordance with this observation, emission from substate II dominates at higher temperatures, while the transition III → 0 only occurs as a shoulder. The 0−0 transition between the lowest triplet substate I and the ground state is very weak, i.e. it is largely forbidden, but it can be detected at low temperatures in excitation (very

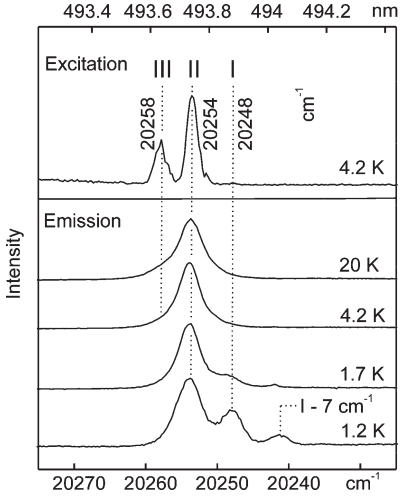

Figure 4. Emission and excitation spectra of Pt(dpyb)Cl in *n*-octane at selected temperatures. For the excitation spectrum, the emission was detected at an energy of 19 570 cm^{-1}, which corresponds to a vibrational satellite of the transition II → 0 (684 cm^{-1} vibration). The emission spectra were recorded under UV excitation ($\lambda_{exc} = 355$ nm).

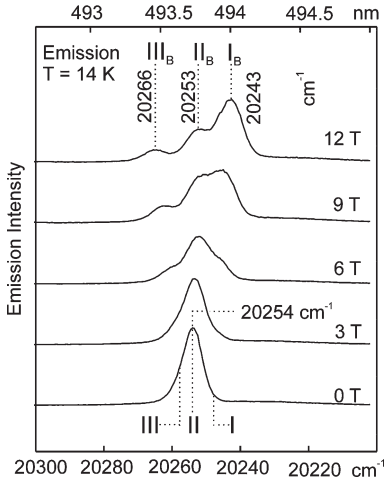

Figure 5. Emission spectra of Pt(dpyb)Cl in *n*-octane at different magnetic field strengths after UV excitation at 355 nm. The temperature of 14 K was chosen to provide a sufficient thermal population of all three substates, being separated by 23 cm^{-1} at $B = 12$ T. The assignment of the three 0−0 transitions at $B = 0$ T results from the temperature-dependent emission and excitation measurements depicted in Figure 4.

(37) Shpol'skii, E. V. *Sov. Phys. Usp.* (*Engl. Transl.*) **1960**, *3*, 372.
(38) Rausch, A. F.; Thompson, M. E.; Yersin, H. *Chem. Phys. Lett.* **2009**, *468*, 46.

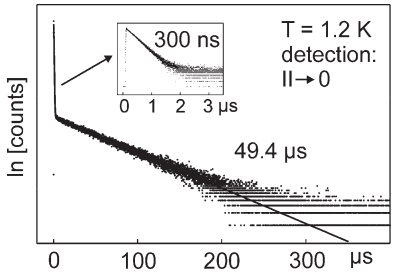

Figure 6. Emission decay curve of Pt(dpyb)Cl in *n*-octane at $T = 1.2$ K after UV excitation at 355 nm. The emission was detected at the electronic 0−0 transition II → 0 (20 254 cm^{-1}).

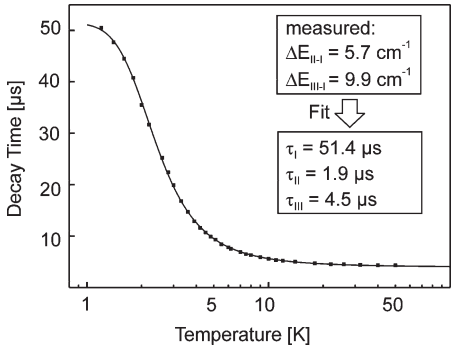

Figure 7. Thermalized emission decay of Pt(dpyb)Cl in *n*-octane versus temperature after pulsed UV excitation at 355 nm. The emission was detected at the electronic 0−0 transition II → 0 (20 254 cm^{-1}). The solid line represents a fit of eq 1 to the experimental data.

weak) and in emission at 20248 cm^{-1}. At $T = 1.2$ K, an additional line at lower energy is observed, which is assigned to correspond to a 7 cm^{-1} local phonon mode (low energy vibration of the dopant in its matrix cage) occurring only in the emission of substate I. It will be shown below that the relatively high intensity of the emisson line II → 0 at 1.2 K is not ascribed to thermal population according to a Boltzmann distribution, but is a consequence of relatively slow processes of spin−lattice relaxation between the substates II and I at that temperature. The spectra depicted in Figure 4 allow the zero-field splitting parameters of the emitting triplet to be determined as $\Delta E_{II-I} = 5.7$ cm^{-1} and $\Delta E_{III-I} = 9.9$ cm^{-1}.

For a further verification of the assignment of the observed lines as representing the electronic origins of the T_1 substates of one single site, emission measurements under the influence of high external magnetic fields have been carried out (Figure 5).

Due to the Zeeman effect, the wave functions of the three T_1 sublevels significantly mix with increasing *B*-fields, leading to distinct changes in the emission spectra. The total splitting, amounting to 10 cm^{-1} at $B = 0$ T, grows to 23 cm^{-1} at $B = 12$ T. Moreover, the radiative allowedness is redistributed between the substates. With increasing *B*-field strength, the emission from the lowest *B*-field disturbed substate I(*B*) becomes dominant while the transition II(*B*) → 0, mainly governing the emission spectrum at zero field, distinctly loses intensity. This behavior shows that the magnetic field drastically alters the properties of the respective 0−0 transitions. Further, the observed Zeeman splitting pattern is a proof that the lines ascribed as substates I, II, and III in Figure 4 really belong to the T_1 state of one single site.

3.4. Thermalized Emission Decay and Energy Level Diagram. The different oscillator strengths of the transitions I ↔ 0, II ↔ 0, and III ↔ 0 manifest themselves also in the emission decay times of the respective T_1 substates. The emission decay curve for a detection energy of 20 254 cm^{-1} (electronic 0−0 transition II → 0) measured at $T = 1.2$ K is shown in Figure 6. A biexponential curve with time constants of 300 ns and 49.4 μs is observed. The long component represents the thermalized emission decay from the three T_1 substates (mainly of substate I), while the short component stems from substate II, determined mainly by its relaxation to substate I. This so-called spin−lattice relaxation (SLR)[28,39,40] is further discussed below.

The individual emission decay times of all three substates to the ground state can be determined from the temperature dependence of the thermalized emission decay. In Figure 7, the measured values are plotted versus temperature for the range $1.2 \leq T \leq 50$ K. For a system of three thermally equilibrated excited states, the rate constant for the depopulation k_{therm}, representing the inverse of the measured decay time τ_{therm}, is given by the expression[33,40−42]

$$k_{therm} = \frac{1}{\tau_{therm}} = \frac{k_I + k_{II}\exp\left(\frac{-\Delta E_{II-I}}{k_B T}\right) + k_{III}\exp\left(\frac{-\Delta E_{III-I}}{k_B T}\right)}{1 + \exp\left(\frac{-\Delta E_{II-I}}{k_B T}\right) + \exp\left(\frac{-\Delta E_{III-I}}{k_B T}\right)} \quad (1)$$

wherein $k_i = 1/\tau_i$ (i = I, II, III) is the rate constant for the depopulation of substate i to the ground state. ΔE_{II-I} and ΔE_{III-I} represent the energy separations between the respective substates. For a fit of eq 1 to the experimental data, the energy separations of $\Delta E_{II-I} = 5.7$ cm^{-1} and $\Delta E_{III-I} = 9.9$ cm^{-1} that result from highly resolved spectra (see section 3.3) were kept constant. The fitting procedure gives the individual decay times of the T_1 substates of $\tau_I = 51.4$ μs, $\tau_{II} = 1.9$ μs, and $\tau_{III} = 4.5$ μs. The value obtained for τ_I is slightly longer than the measured decay time at 1.2 K (Figure 6), since the substates I and II are already slightly thermalized even at this low temperature. Interestingly, the obtained rate constant ratio k_{II}/k_{III} of 2.4 is in good agreement with the ratio of 2.3 as determined in section 3.3 from the electronic 0−0 transitions in the excitation spectrum. This indicates comparable radiative and nonradiative deactivation mechanisms for both substates.

At $T = 1.2$ K, the spin−lattice relaxation between the substates I and II of Pt(dpyb)Cl in *n*-octane is dominated by the *direct process*, describing a resonant one-phonon transition.[28,39,40,43] For a determination of the SLR time, one has to take into account that substate II is

(39) Strasser, J.; Homeier, H. H. H.; Yersin, H. *Chem. Phys.* **2000**, *255*, 301.
(40) Yersin, H.; Strasser, J. *Coord. Chem. Rev.* **2000**, *208*, 331.
(41) Harrigan, R. W.; Crosby, G. A. *J. Chem. Phys.* **1973**, *59*, 3468.
(42) Azumi, T.; O'Donnell, C. M.; McGlynn, S. P. *J. Chem. Phys.* **1966**, *45*, 2735.
(43) Scott, P. L.; Jeffries, C. D. *Phys. Rev.* **1962**, *127*, 32.

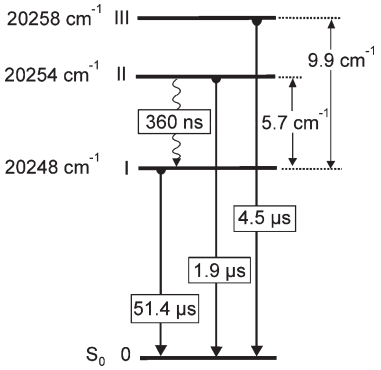

Figure 8. Energy level diagram and decay times of the T_1 substates of Pt(dpyb)Cl in *n*-octane. The value of $\tau_{SLR} = 360$ ns applies to $T = 1.2$ K.

depopulated by relaxation to substate I, given by the SLR rate $k_{SLR} = (\tau_{SLR})^{-1}$, and by a radiative and nonradiative relaxation to the ground state 0, given by the usual decay rate $k_{II} = (\tau_{II})^{-1}$. Thus, the experimentally determined decay rate (short decay component) can be expressed by[28,38−40]

$$k_{II}^{exp} = \frac{1}{\tau_{II}^{exp}} = k_{SLR} + k_{II} \qquad (2)$$

With $\tau_{II}^{exp} = 300$ ns (Figure 6) and $k_{II} = (\tau_{II})^{-1} = (1.9\ \mu s)^{-1}$; a value of $\tau_{SLR} = 360$ ns is found for $T = 1.2$ K.

The results discussed above are summarized in an energy level diagram for the T_1 substates as shown in Figure 8.

The energy separation of $\Delta E_{III-I} \approx 10$ cm^{-1}, that is the total zero-field splitting, can be used to classify the emitting triplet state. This value characterizes the amount of MLCT character and the importance of spin−orbit coupling for the emitting triplet state via the involved d-orbital admixtures. According to an empirical ordering scheme,[8,26−28,40] a triplet state which exhibits a value of $\Delta E(ZFS) \approx 10$ cm^{-1} can be assigned as being largely of ligand-centered (^{3}LC, $^3\pi\pi^*$) character, though with moderate MLCT (5dπ^*) perturbations. The extremely weak allowedness observed for the transition 0 → I (Figure 4) and the relatively long decay time of $\tau_I = 51.4$ μs indicate that substate I exhibits almost pure triplet character, while the substates II and III with $\tau_{II} = 1.9$ μs, $\tau_{III} = 4.5$ μs, and much higher allowednesses for the respective absorptions from the ground state (Figure 4) contain significantly larger admixtures of higher-lying ^{1}MLCT states.

3.5. Vibrational Satellite Structures. Beside the electronic 0−0 transitions, the vibrational satellite structures in the highly resolved emission spectra of Pt(dpyb)Cl in *n*-octane are also very informative with respect to the different properties of the triplet substates. In particular, the vibrational satellite structure in the emission of substate I differs strongly from the satellite structure in the emission of the substates II and III. In Figure 9, the electronic 0−0 transitions and the vibrational satellites corresponding to ground state modes are depicted for the temperatures of 1.2 and 4.2 K.

Many of the satellites observable in Figure 9 correspond to fundamentals. Low energy modes (with energies up to ≈100 cm^{-1}) are largely determined by vibrations of

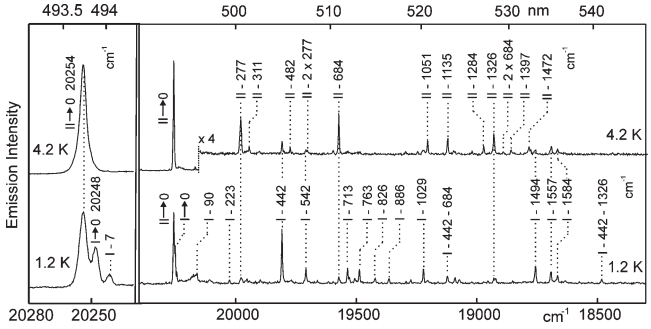

Figure 9. Time-integrated emission spectra of Pt(dpyb)Cl in *n*-octane at $T = 1.2$ and 4.2 K after UV excitation at 355 nm. Note the scaling factor in the 4.2 K spectrum. The region of the electronic 0−0 transitions is additionally depicted on an enlarged scale.

the dopant in its matrix cage, which represent so-called local phonon modes. It should be noticed that a mixing of internal low-energy vibrations of the complex with such local phonon modes is still relevant up to ≈150 cm^{-1}.[44] Overlapping with this energy range up to 500/600 cm^{-1}, metal−ligand (M-L) vibrations are found, while fundamentals higher than ≈600 cm^{-1} can usually be assigned as internal ligand modes.[28] As already substantiated in the discussion of the electronic 0−0 transitions in section 3.3, the spectrum at 4.2 K is dominated by emission from T_1 substate II. Due to the short decay time (relatively high allowedness) of the transition to the singlet ground state and the appearance of (weak) overtone satellites for the most intense fundamentals (e.g., 277, 684, 1135, and 1326 cm^{-1}), many of the vibrational satellites observed at 4.2 K can be assigned to correspond to totally symmetric Franck−Condon (FC) active modes.[28,45−47]

For those modes showing second members of vibrational progressions, one can determine the so-called Huang−Rhys parameter S, which is specific for each vibrational mode and depends on the shift ΔQ of the equilibrium positions of the involved electronic states for the corresponding vibrational coordinate.[28,45−47] A Huang−Rhys parameter of zero corresponds to equal geometries of the excited state and the ground state. In this case, the whole emission intensity is carried by the electronic 0−0 transition. With an increase of the displacement ΔQ, and thus an increase of S, the intensity of the electronic 0−0 line decreases and the vibrational satellites of the respective Franck−Condon progression gain intensity. In the low-temperature limit, the Huang−Rhys parameter for a specific mode does not depend on the vibrational energy[45] and can be determined by using the expression[28,47,48]

$$S = v\frac{I_v}{I_{v-1}} \qquad (3)$$

(44) Becker, D.; Yersin, H.; von Zelewsky, A. *Chem. Phys. Lett.* **1995**, *235*, 490.
(45) Henderson, B.; Imbusch, G. F. *Optical Spectroscopy of Inorganic Solids*; Clarendon: Oxford, 1989.
(46) Ballhausen, C. J. *Molecular Electronic Structures of Transition Metal Complexes*; McGraw-Hill: New York, 1979.
(47) Solomon, E. I. *Comments Inorg. Chem.* **1984**, *3*, 300.
(48) Seiler, R.; Kensy, U.; Dick, B. *Phys. Chem. Chem. Phys.* **2001**, *3*, 5373.

wherein v is the vibrational quantum number and I_v is the intensity of the respective member of the Franck−Condon progression. In the case of Pt(dpyb)Cl in *n*-octane at 4.2 K, most of the emission intensity is carried by the electronic 0−0 transition II → 0, while the satellites stemming from vibrational modes are very weak. For the FC modes with fundamental energies of 277, 684, 1135, and 1326 cm^{-1} (see above), a Huang−Rhys parameter of $S \approx 0.1$ is found. A value of that magnitude shows that only very small geometry changes occur between the singlet ground state and the emitting T_1 state, at least in a rigid n-octane matrix at cryogenic temperatures.

For weaker satellites, second members of progressions cannot be observed; presumably, they are hidden in the noise of the spectrum due to small Huang−Rhys parameters.

A temperature increase to, e.g., 10 K does not lead to significant changes in the emission spectrum (not shown). Thus, in particular, the same vibrational satellites as found in the emission of substate II occur also in the emission of substate III. This behavior supports the results as presented already in section 3.4 concerning the similar deactivation mechanisms of the two substates.

At $T = 1.2$ K, the emission mainly stems from the lowest triplet substate I, which carries a much lower allowedness with respect to the electronic 0−0 transition to the ground state as compared to substate II. Thus, substate I can be deactivated by a different vibrational mechanism, and a completely different situation is found. Many intense vibrational satellites observed in the emission of substate I are absent in the emission spectrum of substate II at 4.2 K. Moreover, one of these satellites is even more intense than the corresponding electronic 0−0 transition I → 0 (442 cm^{-1} mode). Obviously, the radiative deactivation at the purely electronic transition is less efficient than the radiative deactivation involving vibrational modes. Further, for these fundamentals, no progressions occur, while some of the most intense Franck−Condon modes (identified in the emission of substate II) form combinations with the intense 442 cm^{-1} mode observed in the emission spectrum of the substate I (e.g., 442 + 684 cm^{-1}, 442 + 1326 cm^{-1}). In analogy to the extensive investigations carried out with Pt(2-thpy)$_2$,[27,28,49] Pt(4,6-dFppy)(acac),[26,29] and $[Os(bpy)_3]^{2+}$,[50] it can be concluded that the observed vibrational satellite structure stemming from substate I is mainly induced by processes of vibronic coupling of substate I to higher lying states via spin-vibronic mechanisms (details are discussed in refs 27 and 28). This type of coupling, frequently called Herzberg−Teller (HT) coupling,[46,51,52] is of particular importance, if the electronic 0−0 transition is largely spin-forbidden and carries only low allowedness. Spin-vibronic coupling becomes effective by modulation of spin−orbit coupling through an adequate vibration along a specific normal coordinate Q of a complex. As a consequence, intensity is induced to the corresponding vibrational satellite with the vibrational energy $\bar{\nu}_Q$, but not to the purely electronic transition.[28,46,52] The satellites

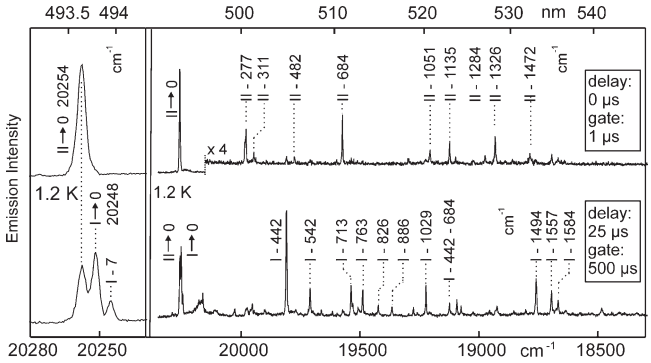

Figure 10. Time-resolved emission spectra of Pt(dpyb)Cl in *n*-octane at $T = 1.2$ K after UV excitation at 355 nm. The short-time spectrum was recorded immediately after the exciting laser pulse in a time window of 1 μs. For the delayed spectrum, a time delay of 25 μs and a time window of 500 μs were chosen. Note the scaling factor in the short-time spectrum. The region of the electronic 0−0 transitions is additionally depicted on an enlarged scale.

of HT active vibrational fundamentals represent so-called "false origins". Indeed, this behavior is observed for the T_1 substate I of Pt(dpyb)Cl in *n*-octane.

Moreover, the substates I and II exhibit distinctly different emission decay times (see section 3.4). Therefore, a separation of the individual spectra of the substates on the time domain is possible and provides deeper insight. Figure 10 shows emission spectra at $T = 1.2$ K which were recorded with different delay times after the exciting laser pulse and in different time windows for detection.

The spectrum obtained immediately after excitation in a time window of 1 μs (compare the fast decay component displayed in Figure 6) is very similar to the time-integrated spectrum obtained at 4.2 K. No other electronic 0−0 transition beside II → 0 is observable. Further, the vibrational satellite structure stems almost exclusively from the fast decaying T_1 substate II. On the other hand, after a delay time of 25 μs, the obtained spectrum is comparable to the time-integrated emission at 1.2 K and is dominated by the emission of substate I. However, substate II also emits in the delayed spectrum, but less intensely than in the time-integrated spectrum (compare the intensity ratios of the electronic 0−0 transitions in Figures 9 and 10). Since processes of spin−lattice relaxation (with $\tau_{SLR} = 360$ ns) can be neglected after a delay time of 25 μs and the initial population of substate II has completely decayed, it can be concluded that the emission from this substate in the delayed spectrum stems only from thermal repopulation according to a Boltzmann distribution.

4. Assignments and Conclusions

This study shows that high-resolution optical spectroscopy at cryogenic temperatures in an *n*-octane matrix allows a detailed characterization of the emitting triplet state of the highly luminescent compound Pt(dpyb)Cl. A total zero-field splitting of the emitting triplet state of $\Delta E(ZFS) = 9.9$ cm^{-1} is observed (see Figure 8). In general, ligand-centered triplet states (^{3}LC states) in organo-transition metal compounds exhibit $\Delta E(ZFS)$ values smaller than 1 cm^{-1}, while for MLCT emitters the splitting can reach a value up to 200 cm^{-1}.[8,27,28,40,50] Thus, it is indicated that the lowest

(49) Wiedenhofer, H.; Schützenmeier, S.; von Zelewsky, A.; Yersin, H. *J. Phys. Chem.* **1995**, *99*, 13385.
(50) Yersin, H.; Kratzer, C. *Coord. Chem. Rev.* **2002**, *229*, 75.
(51) Herzberg, G.; Teller, E. Z. *Z. Phys. Chem.* **1933**, *B21*, 410.
(52) Fischer, G. *Vibronic Coupling*; Academic Press: London, 1984.

triplet of Pt(dpyb)Cl can be described as being largely ligand-centered with moderate metal-to-ligand charge transfer character mixed in. This is in accordance with the relatively short individual decay times of the higher-lying T_1 substates II and III, which mainly govern the emission properties at ambient temperature. For compounds with emitting states of ^{3}LC character, direct spin−orbit coupling to higher-lying singlet and triplet MLCT states is weak. However, the admixture of such states, which is necessary to obtain a considerable magnitude of ZFS and relatively short substate decay times, can proceed via a two-step mechanism involving configuration interaction of the ^{3}LC substates with the substates of higher lying ^{3}MLCT states. These latter states allow direct spin−orbit coupling with other ^{1,3}MLCT states. It is stressed that only MLCT states which involve different metal d-orbitals can mix via direct SOC. (For details see refs 26, 27, 29, 53, and 54.)

Another parameter to characterize the nature of the emissive triplet state is given by the Huang−Rhys parameter S. For compounds with ligand-centered T_1 states, such as $Pd(2\text{-thpy})_2$,[28] $[Pt(bpy)_2]^{2+}$,[55] or $[Rh(bpy)_3]^{3+}$ [56] (all of which exhibit $\Delta E(ZFS)$ values of $< 1\ cm^{-1}$), the maximum S values are as large as ≈ 0.3, while for a typical MLCT emitter, such as $[Os(bpy)_3]^{2+}$ (with $\Delta E(ZFS) = 211\ cm^{-1}$),[57] the maximum Huang−Rhys parameter amounts to only 0.08. The occurrence of significantly smaller S parameters for compounds with emitting triplet states of MLCT character than for compounds with emitting states of ^{3}LC origin is ascribed to the more distinct spatial extensions of the electronic wave functions over the ligands and the metal with increasing MLCT admixture.[28,58,59] In this situation, an electronic transition results in a smaller charge density change per ligand and thus has less influence on the specific bonding properties (small ΔQ values).[8,28]

For the compounds Pt(4,6-dFppy)(acac)[26] and Pt(ppy)-(acac),[60] which exhibit similar zero-field splittings and thus similar MLCT character in the emitting states as in Pt-(dpyb)Cl, Huang−Rhys parameters of $S \approx 0.2$ were determined for prominent FC modes. The smaller S values for Pt(dpyb)Cl of only ≈0.1, or the smaller geometry changes between S_0 and T_1, are ascribed to the higher rigidity of the Pt(N^C^N) system with a terdentate ligand compared to the related Pt(N^C) compounds with bidentate phenylpyridine-type ligands. In the latter ones, the plane of the N^C ligand can potentially twist relative to the plane containing the other two ligating atoms and, thus, can give rise to additional distortions.

At ambient temperature in fluid solution, larger values of the Huang−Rhys parameters are observed. In this situation of a "soft" environment, the displacements ΔQ of the potential energy surfaces of the excited electronic state can be assumed to be larger than in a rigid (poly)crystalline host cage at 4.2 K. The temperature dependence of S can be neglected in this respect, since, for vibrational fundamentals with energies between 1000 and 1500 cm^{-1}, the low-temperature approximation of the Huang−Rhys parameter is still valid at 300 K.[61] Interestingly, the trends for the S values found from highly resolved spectra at cryogenic temperatures are still maintained in fluid solution under ambient conditions. For Pt(dpyb)Cl, the 300 K electronic origin band is dominant and significantly more intense than the vibrational satellite bands which stem from (overlapping) intraligand fundamentals, combinations, and/or progressions. In *n*-octane, the intensity of the most intense vibrational satellite band amounts to ≈0.5 relative to the electronic origin peak (see Figure 3), while for Pt(II) compounds with bidentate phenylpyridine-type ligands, a much larger portion of the emission intensity is found in the range of the vibrational satellite bands.[62−64] For Pt(4,6-dFppy)(acac) in *n*-octane, for example, the emission intensity of the most intense vibrational satellite band relative to the intensity of the origin band is as large as ≈0.8.[38]

These presented results are highly important with respect to color purity requirements for OLEDs. Especially in the blue spectral region, Pt(N^C^N) systems can achieve higher emission color purity than related Pt(N^C) compounds, since in the former ones the intensity contributions of the green-to-yellow low-energy vibrational satellite bands are strongly reduced.[64] These aspects will, in combination with the higher emission quantum yields and relatively short emission decay times of this class of Pt(II) complexes with terdentate ligands, allow the development of OLEDs with further improved device characteristics.

Note added in Proof: A recent related paper by Tong and Che was published.[65]

Acknowledgment. The Bundesministerium für Bildung und Forschung (BMBF) is gratefully acknowledged for providing the funding of this investigation. We thank the British Council and the German Academic Exchange Service (DAAD) for a bilateral ARC travel grant, the COST project for financial support within the project D35-0010-05, and the University of Durham for a doctoral fellowship to L.M.

(53) Miki, H.; Shimada, M.; Azumi, T.; Brozik, J. A.; Crosby, G. A. *J. Phys. Chem.* **1993**, *97*, 11175.
(54) Azumi, T.; Miki, H. *Top. Curr. Chem.* **1997**, *191*, 1.
(55) Humbs, W.; Yersin, H. *Inorg. Chim. Acta* **1997**, *265*, 139.
(56) Humbs, W.; Yersin, H. *Inorg. Chem.* **1996**, *35*, 2220.
(57) Yersin, H.; Humbs, W.; Strasser, J. *Top. Curr. Chem.* **1997**, *191*, 153.
(58) Maestri, M.; Sandrini, D.; Balzani, V.; von Zelewsky, A.; Deuschel-Cornioley, C.; Jolliet, P. *Helv. Chim. Acta* **1988**, *71*, 1053.
(59) Moore, J. J.; Nash, J. J.; Fanwick, P. E.; McMillin, D. R. *Inorg. Chem.* **2002**, *41*, 6387.
(60) Rausch, A. F. Ph.D. thesis, Universität Regensburg, in preparation
(61) For a vibrational mode with an energy in the range of 1000−1500 cm^{-1}, a low-temperature Huang−Rhys parameter of 0.1 increases only marginally to ≈0.1001−0.101 at 300 K (compare ref 45, p 206).
(62) Brooks, J.; Babayan, Y.; Lamansky, S.; Djurovich, P. I.; Tsyba, I.; Bau, R.; Thompson, M. E. *Inorg. Chem.* **2002**, *41*, 3055.
(63) Ghedini, M.; Pugliese, T.; La Deda, M.; Godbert, N.; Aiello, I.; Amati, M.; Belviso, S.; Lelj, F.; Accorsi, G.; Barigelletti, F. *Dalton Trans.* **2008**, *32*, 4303.
(64) Yang, X.; Wang, Z.; Makaduni, S.; Li, J.; Jabbour, G. E. *Adv. Mater.* **2008**, *20*, 2405.
(65) Tong, G. S.-M.; Che, C.-M. *Chem.—Eur. J.* **2009**, *15*, 7225.